Journal Pre-proof

Dielectric properties and thermal behavior of electrolytic manganese anode mud in microwave field

Kangqiang Li, Jin Chen, Jinhui Peng, Roger Ruan, Mamdouh Omran, Guo Chen

PII: S0304-3894(19)31181-1

DOI: https://doi.org/10.1016/j.jhazmat.2019.121227

Reference: HAZMAT 121227

To appear in:

Received Date: 14 July 2019

Revised Date: 11 September 2019

Accepted Date: 12 September 2019

Please cite this article as: Li K, Chen J, Peng J, Ruan R, Omran M, Chen G, Dielectric properties and thermal behavior of electrolytic manganese anode mud in microwave field, *Journal of Hazardous Materials* (2019), doi: https://doi.org/10.1016/j.jhazmat.2019.121227

Dielectric properties and thermal behavior of electrolytic manganese anode mud in microwave field

Kangqiang Li [a], Jin Chen [a, **], Jinhui Peng [a, b], Roger Ruan [b, d], Mamdouh Omran [e], Guo Chen [a, b, c, *]

[a] *Key Laboratory of Unconventional Metallurgy, Ministry of Education, Faculty of Metallurgical and Energy Engineering, Kunming University of Science and Technology, Kunming 650093, P.R. China.*

[b] *Key Laboratory of Green-Chemistry Materials in University of Yunnan Province, Yunnan Minzu University, Kunming 650500, P.R. China.*

[c] *Hunan Provincial Key Laboratory of Efficient and Clean Utilization of Manganese Resources, Central South University, Changsha 410083, Hunan, P.R. China.*

[d] *Center for Biorefining, Bioproducts and Biosystems Engineering Department, University of Minnesota, 1390 Eckles Ave., Saint Paul, MN 55108, USA.*

[e] *Process Metallurgy Research Group, Faculty of Technology, University of Oulu, Finland.*

[*] Corresponding author: Tel: +86-871-65138997; Fax: +86-871-65138997

E-mail address: guochen@kmust.edu.cn

[**] Co-Corresponding author: Tel: +86-871-65138997; Fax: +86-871-65138997

E-mail address: jinchen@kmust.edu.cn

The main highlights of this work are as follows,

•Investigation of the dielectric properties of manganese anode mud.

•Evaluation of the thermal behavior of manganese anode mud in microwave field.

•Declaration of the feasibility of applying microwave heating to manganese anode mud.

Abstract

Exploring the dielectric properties of a material can provide guidance for applications of microwave technology to the material. In this work, dielectric properties and thermal behavior of manganese anode mud and pure MnO_2, $CaSO_4$ and $PbSO_4$ components were systematically investigated. Results indicated that manganese anode mud showed excellent responsiveness to microwaves, with ε_r' value of 17.971 (F/M) at room temperature and a maximum value of 20.816 (F/M) at 150 °C, rendering it took only 5.5 min for manganese anode mud to be heated from room temperature to 1000 °C. The dielectric properties of manganese anode mud were related to its thermal behavior, mainly affected by MnO_2 component. Moreover, the heating process of manganese anode mud was divided into four stages identified by temperatures: less than 200 °C, 200 °C-700 °C, 700 °C-900 °C, greater than 900 °C, corresponding to the five stages of thermal behavior: the removal of absorption water and combined water, the decomposition reaction of $Pb_2Mn_8O_{16}$, and the deoxidation reactions of PbO_2, MnO_2 and

Mn_3O_4. The work highlights the feasibility of processing manganese anode mud by microwave heating.

Keywords: manganese anode mud; dielectric properties; heating characteristics; thermochemical behavior; microwave heating

1 Introduction

Manganese and its related processing products are widely applied in various fields of the national economy, predominantly as deoxidizer, desulfurizer, and alloying agent in the steelmaking process [1-2], additionally consumed in nonferrous metallurgy, chemical, electronics, battery, agriculture, and national defense etc. [3-7]. Manganese metal is primarily produced by electrolysis, therefore the increased demand for manganese alloys has promoted the rapid development of electrolytic manganese industry [8]. However, in the process of electrolytic manganese production, it is inevitable to generate a large amount of waste residue in the anode region of the electrolytic cell, namely the electrolytic manganese anode mud [9]. As a hazardous material, the component compositions of manganese anode mud are complex, with 40% to 50% of high manganese (Mn) content and 6%-7% of high lead (Pb) content, even accompanying with other complicated impurities such as Co, Ni, Fe, Pb, Sn, and other soluble salts [10]. With the low activity and complex compositions, manganese anode mud cannot be directly recycled by simple mechanical or mineral processing methods, mainly stored as hazardous waste or sold cheaply, with only a small part used for steelmaking additives and most of the anode mud not fully utilized, rendering waste of resources and environmental pollution [11]. Currently, among the reported technologies for comprehensive

utilization of electrolytic manganese anode mud, reduction roasting-leaching method [12] and wet reduction-leaching method [13] are the mainly widely applied methods, aiming at the recycle utilization of manganese (Mn) and lead (Pb), while without considering the crystal structure advantage of manganese dioxide (MnO_2) in manganese anode mud and involving the secondary pollution control of lead (Pb), even the fabrication and environmental applications of multifunctional mixed metal-biochar composites [14-16]. Moreover, the methods are plagued with high temperature, high-energy consumption, environmental restrictions, complicated operation, and lengthy process; and there are also specific requirements for the reducing agents. If manganese anode mud was disposed improperly, serious heavy metal pollution accidents and resources waste will be caused. Therefore, it urgently demands development of new processes that are potentially environmentally benign and cost effective to process manganese anode mud.

Microwave heating (2450 MHz) as a novel green method, has become increasingly frequent in the fields, including mineral processing, organic synthesis, material preparation, and environmental remediation, etc. [17-22]. Actually, in the comprehensive utilization of hazardous waste resources, Saucier et al. reported the efficient removal of sodium diclofenac (DFC) and nimesulide (NM) from aqueous solutions with activated carbon, prepared from cocoa shell by microwave-induced chemical activation process [23]. Leonelli et al. utilized microwave technology to successfully inert asbestos containing waste (ACW) [24]. The essence of microwave heating is by generating dielectric loss in the interior of the material, and then through the dielectric loss to directly transfer microwave energy to the reacting molecules or atoms inside the material, therefore rendering microwave heating more efficient

than conventional heating [25-27].

The ability of a material to absorb microwaves depends primarily on its dielectric properties, which are affected by the frequency of the electric field, temperature, moisture content and chemical composition etc., wherein temperature is particularly important. Ye et al. [28] and Li et al. [29] investigated the high-temperature dielectric properties of waste hydrodesulfurization catalysts and manganese ore-walnut shell mixtures, respectively, indicating that temperature has significant influence for dielectric properties of materials. Therefore, before performing microwave technology processing, it is the basis to determine the responsiveness of a material to microwaves, referring to the dielectric properties of materials at high temperatures. Moreover, based on the above microwave heating mechanism, it could be speculated that microwave technology can be applied efficiently to process manganese anode mud, attributed to that manganese anode mud contained various metal compounds, which show excellent microwave-absorbing ability [30].

Previous work focused on the reduction-leaching of manganese (Mn) and lead (Pb) from manganese anode mud by conventional heating, and Tokkan et al. have investigated the silver removal from anode slime by microwave irradiation [31], while few detailed studies reported that microwave heating technology directly acts on manganese anode mud to replace conventional heating, instead of microwave radiation, even the analysis about the dielectric properties and thermal behavior of manganese anode mud. Moreover, to make microwave heating technology more efficient apply to manganese anode mud, before microwave heating processing, it is fundamentally important to determine the high-temperature dielectric properties of manganese anode mud. Hence, in the present work, the dielectric properties and

heating characteristics of manganese anode mud in microwave field were evaluated to clarify the feasibility of processing manganese anode mud through microwave heating; ultimately, the dielectric properties and heating characteristics of three pure components in manganese anode mud were studied to elucidate effects of various components on the dielectric properties and heating characteristics of manganese anode mud, including MnO_2, $CaSO_4$, and $PbSO_4$; moreover, the thermochemical characteristics of manganese anode mud were investigated to understand the thermal decomposition behavior of manganese anode mud, further contributing to analyze the process mechanism of manganese anode mud in microwave field.

2 Experimental

2.1 Materials and chemical reagents

Electrolytic manganese anode mud was used as raw material, received from CITIC Dameng Mining Industries Limited (Nanning City, Guangxi Province, P.R. China). The chemical compositions of manganese anode mud were provided by Advanced Analysis and Measurment Center of the Yunnan University, as presented in Table 1. It was characterized by the manganese anode mud with high manganese content (Mn, 57.58%) and high lead content (Pb, 6.06%). Fig. 1 illustrated the XRD pattern of manganese anode mud, analyzed by X-ray diffractometer (X'Pert3 powder, Panaco, Netherlands); and it indicated the manganese anode mud contained MnO_2 phase (JCPDS: 44-0140), $PbSO_4$ phase (JCPDS: 36-1461), $CaSO_4$ phase (JCPDS: 45-0157), $Pb_2Mn_8O_{16}$ phase (JCPDS: 29-0778).

Based on the phase compositions from XRD analysis, three chemical reagents (including

MnO_2, $CaSO_4$, and $PbSO_4$) were acquired to analyze its effect on the dielectric properties and thermal behavior of manganese anode mud in microwave field, while with $Pb_2Mn_8O_{16}$ no purchase channel. Wherein MnO_2 (85.0%) and $CaSO_4 \cdot 2H_2O$ (99.0%) were purchased from Fengchuan Chemical Reagent Technologies Co., Ltd (Tianjin City, P.R. China); $PbSO_4$ (98.0%) was purchased from Macklin Biochemical Co., Ltd (Shanghai City, P.R. China); meanwhile, all the chemical reagents were analytically pure.

2.2 Measurement instrumentations for dielectric properties and heating characteristics

The schematic diagram of measurement instrumentations for dielectric properties and heating characteristics was illustrated in Fig. 2, wherein Fig. 2(a) presented the dielectric test device, and Fig. 2(b) demonstrated the microwave box furnace, respectively.

The measurement of the dielectric properties was performed by cylindrical cavity perturbation method with a dielectric test device (Agilent-E5071C, MYWAVE), with a variable-temperature test system for complex permittivity measurements of powdered solid materials. As shown in Fig. 2(a), the device mainly consisted of a cylindrical resonant cavity (TM_{0n0}), coupling device, temperature test instrument, eddy current heating system, circulating water cooling system, detector and DSP, interface circuit, vector network analyzer (Agilent-N5230C), computer and oil-free-air compressor.

The heating characteristics of manganese anode mud and three pure components were determined by a microwave box furnace (HM-X08-16, MAKEWAVE), with a K-type thermocouple (ZS5.K-T03T) serviced with a maximum temperature of 1200 °C. As shown in Fig. 2(b), the microwave furnace was mainly composed by microwave reactor, rotation, motor, thermocouple, insulating brick, vacuum pump, a computer control system, rotameter,

flowmeter and gas generator. Continuous controllable microwave power was provided by two magnetrons at 2.45 GHz microwave frequency and 3 kW microwave power. The reactor was cooled by water circulation when working.

2.3 Measurement procedure of dielectric properties and heating characteristics

Manganese anode mud were ground and screened to particle size ranges of 60-140 mesh, with a median particle diameter (D_{50}) of 5.85 μm, examined by a laser particle size analyzer (JL-1177, Chengdu Jingxin Powder Analyse Instruments Co. Ltd). Before testing and characterizing, the anode mud specimens were dried at 105 °C for 12 h in an air dry oven (DHG9079A, Shanghai YiHeng Scientific Instruments Co. Ltd). After drying, each of the samples was subjected to the high temperature TGA thermogravimetric analyzer (TGA/DSC 1/1600, METTLER TOLEDO, Switzerland) by placing 5.0 mg sample in a ceramic crucible with alumina (70 μL) as the sample holder and measured at the temperature range from 25 °C to 1000 °C with Air flow rate of 50.0 mL/min, at different heating rates of 10 K/min, 20 K/min, 30 K/min, respectively. In addition, certain weight of manganese anode mud and three pure components were placed into corundum crucible and then introduced into the microwave box furnace to measure microwave heating characteristics, under microwave irradiation at 2450 MHz from room temperature to 1000 °C with air atmosphere; wherein 30.0 g of manganese anode mud was measured at three microwave powers with 1000 W, 1200 W, and 1400 W; and 40.0 g of the three pure components were determined at 1200 W.

The dried specimens were also introduced to the dielectric test device (Agilent-E5071C, MYWAVE) to measure the complex permittivity of manganese anode mud and the three pure components, from room temperature to 1000 °C, with 50 °C interval as a temperature variable

node. And the complex permittivity of the material can be obtained through four steps by cavity calibration, quartz empty tube calibration, charging and loading quartz tube test, and recalculation of the just measured complex permittivity [28-29]. More detailed information about the dielectric properties was presented in Supplementary material. Two-frequency system of 2450 MHz and 915 MHz was attached to the dielectric device, while microwave equipment applied in laboratory are mostly equipped with a frequency of 2450 MHz, therefore, the dielectric properties of manganese anode mud and the three pure components were measured at 2450 MHz.

3 Results and discussion

3.1Thermogravimetric analysis

Thermogravimetric measurement can determine the thermochemical characteristics of manganese anode mud, further assisting to analyze the dielectric properties and thermal behavior of manganese anode mud in microwave field. Therefore, thermogravimetric analysis for manganese anode mud was conducted at different heating rates, and the TG-DTG-DSC curves were plotted in Fig. 3.

Fig. 3(a) presented the TG curves. It was observed from Fig. 3(a) that at different heating rates, three TG curves showed the same trend for the weight loss of manganese anode mud with temperature, and the thermal behavior of manganese anode mud can be divided into five stages: (1) the first stage, the weight loss at this stage was attributed to the evaporation of absorption water, and the weight loss of manganese anode mud was near 4.0%~5.0% with different heating rates. (2) The second stage, the weight loss could correspond to the dehydration stage of the combined water. Wherein $CaSO_4 \cdot 2H_2O$ phase in manganese anode

mud occur the loss of 1 molecule of combined water at 128 °C and all combined water at 163 °C [32]. (3) The third stage, with temperature improving, the lead manganese oxide $Pb_2Mn_8O_{16}$ was decomposed into PbO_2, MnO_2 and MnO by thermal effect. The weight loss at the stage was assigned to the deoxidation reaction of the decomposed product PbO_2, with the initial temperature of PbO_2 deoxidation reaction being 403.6 °C (the theoretical initial temperature calculated by thermochemical software FactSage and HSC). (4) The fourth stage, the deoxidation reaction of MnO_2 phase led to the weight loss of manganese anode mud at this stage. The main phase composition in manganese anode mud, original MnO_2 phase (concluded from Table 1 and Fig. 1) and the new MnO_2 phase generated by $Pb_2Mn_8O_{16}$ thermal decomposition reaction, were deoxidized into Mn_2O_3 at 529.3 °C, meanwhile with some oxygen gas (O_2) produced [33]. (5) The fifth stage could be commensurate with the deoxidation reaction of Mn_2O_3 phase [33]. Temperature increasing, Mn_2O_3 phase was deoxidized into Mn_3O_4 and O_2 at 999.7 °C [33]. From Fig. 3(a), it was observed that at different heating rates, the weight loss at different stages varied except the first stage, which was attributed to the nearly same content of absorption water of manganese anode mud, after dried at 105 °C for 12 h before testing. Meanwhile, the residue weight of manganese anode mud was close for three heating rates, with 79.66%, 80.95% and 81.91% at 10 K/min, 20 K/min and 30 K/min, respectively. During the weight loss process of manganese anode mud, the decomposition reactions in manganese anode mud occurred at with temperature regimes from 25 °C to 1000 °C, could be summarized as follows,

$$Pb_2Mn_8O_{16}=2PbO_2+4MnO_2+4MnO \quad (3)$$

$$2PbO_2=2PbO+O_2\,(g) \quad (4)$$

$$4MnO_2=2Mn_2O_3+O_2\,(g) \quad (5)$$

$$6Mn_2O_3=4Mn_3O_4+O_2\,(g) \quad (6)$$

The melting point temperature of $PbSO_4$ and $CaSO_4$ phase are 1087 °C and 1450 °C, respectively, which the two melting point temperatures are higher than 1000 °C. Therefore, $PbSO_4$ and $CaSO_4$ phases keep the original form at temperature regime from 25 °C to 1000 °C, without decomposition reaction occurred, further with few contribution to the weight loss of manganese anode mud.

Fig. 3(b) illustrated the DTG curves. It was observed from Fig. 3(b) that the thermal effects of those DTG curves showed the same trend, with four endothermic peaks and two exothermic peaks. The first endothermic peak at nearly 50 °C, was attributed to the evaporative endotherm of absorption water. The second endothermic peak at nearly 250 °C, was caused by the decomposition reaction of lead manganese oxide $Pb_2Mn_8O_{16}$ and the removal of combined water. The first small exothermic peak appeared at closely 330 °C, which was assigned to the crystal transformation of amorphous MnO_2 into β-MnO_2 [34], the sample began to undergo a crystal form transition to release heat, meanwhile offsetting part of the heat required for evaporation of the combined water, therefore, the exothermic peak was not obvious. Another small exothermic peak at 410 °C, was ascribed to the deoxidation reaction of $2PbO_2=2PbO+O_2\,(g)$, which is an exothermic reaction. The third endothermic peak was generated by the deoxidation reaction of $4MnO_2=2Mn_2O_3+O_2\,(g)$ [35], and the four endothermic peak was assigned to the deoxidation reaction of $6Mn_2O_3=4Mn_3O_4+O_2\,(g)$ [35], with both the two endothermic reactions. Moreover, it can be concluded from Fig. 3(b) that those endothermic and exothermic peaks temperature varied with different heating rates, and

the values of those peak temperatures increased with the heating rate.

Fig. 3(c) showed the DSC curves. It can be seen from Fig. 3(c) that those DSC curves show the same trend with an epitaxial termination temperature peak, referring to the intersection of the tangent of the DSC curve and the maximum weight loss line, where the maximum weight loss of manganese anode mud occurred, with 633.9 °C, 681.2 °C, and 720.7 °C at 10 K/min, 20 K/min, and 30 K/min, respectively; indicating decreasing the heating rate will decrease the values of those peak temperatures, which was consistent with the phenomenon observed from DTG curves (Fig. 3(b)), referring to that peaks temperature decreased with the heating rates decreasing.

3.2 Dielectric properties analysis

The dielectric properties (including dielectric constants (ε_r'), dielectric loss factors (ε_r''), and loss tangent coefficients (tan δ)) of manganese anode mud and three pure components were measured, and the results were illustrated in Fig. 4, Fig. 5 and Fig. 6, respectively.

3.2.1 Dielectric constants analysis

Fig. 4 presented the dielectric constants (ε_r'). ε_r' indicates the ability of the substance to absorb microwaves and store electromagnetic waves in matter [28-29]. For manganese anode mud, as shown in Fig. 4(a), the ε_r' value was 17.971 (F/M) at room temperature, and had a downward trend before 50 °C, which was attributed to the removal of absorption water of the anode mud, corresponding to the first dehydration stage of thermogravimetric analysis process. Temperature higher than 50 °C, the ε_r' of manganese anode mud increased with temperature increasing, with the maximum ε_r' value of 20.816 (F/M) at 150 °C. In the temperature ranging from 50 °C to 150 °C, one physical and one chemical process occurred,

wherein the dehydration stage of the combined water caused the decrease of the ε_r' value, meanwhile the decomposition reaction of lead manganese oxide $Pb_2Mn_8O_{16}$ generated PbO_2 and MnO_2, which both show excellent microwave-absorbing properties [30]; hence, in a whole, the ε_r' of manganese anode mud showed an upward tendency at temperature between 50 °C and 150 °C. Temperatures from 150 °C to 400 °C, the ε_r' value gradually decreased with temperature, the decrease of ε_r' value was mainly ascribed to the removal of the combined water. Higher than 400 °C, the ε_r' value was observed to suddenly drop to low levels, with a value of 1.141 (F/M) at 550 °C, which was attributed to the deoxidation reaction of $2PbO_2=2PbO+O_2$ (g), PbO_2 with high dielectric loss was converted to PbO with low high dielectric loss. Moreover, temperature continuously increasing, it increased to 11.614 (F/M) at 700 °C, which was caused by the crystal transformation of amorphous MnO_2 into β-MnO_2, wherein β-MnO_2 with much higher dielectric properties than amorphous MnO_2. The same phenomenon also can be observed from the ε_r' curve of pure MnO_2, with ε_r' value increased to high levels, at temperature ranging from 500 °C to 650 °C (Fig. 4(b)). The decrease of ε_r' value of manganese anode mud between 650 °C to 850 °C, was assigned to the deoxidation reaction of $4MnO_2=2Mn_2O_3+O_2$ (g) [33], and the final decrease of the ε_r' value can be explained by the deoxidation reaction of $6Mn_2O_3=4Mn_3O_4+O_2$ (g) [33], wherein MnO_2 is easily heated by microwaves, while Mn_2O_3 and Mn_3O_4 hardly absorb microwaves, indicating MnO_2 was gradually reduced to weakly microwave-absorbing materials such as Mn_2O_3, and Mn_3O_4, rendering the decrease of the dielectric properties [36]. Meanwhile, the gas produced by deoxidation reactions caused the volume of the sample in the quartz tube to expand, causing a decrease in density and further rendering a decrease in dielectric properties.

The dielectric properties of the three pure components, including MnO_2, $CaSO_4$ and $PbSO_4$, were also determined at the same conditions to explore influence of the three pure components on the dielectric properties of manganese anode mud. For the pure MnO_2, as observed from Fig. 4(b), the ε_r' curve of MnO_2 presented the similar change trend with that of manganese anode mud: rose firstly, and then decreased slightly, followed by increased intensely and finally decreased with temperature. In detail, at temperatures between room temperature to 500 °C, the ε_r' values of MnO_2 fluctuated up and down, but remained at a high level overall, even with a minimum value of 10.359 (F/M) at 500 °C, indicating pure MnO_2 with a good microwave-absorbing property. The fluctuation of ε_r' value at this temperature regime (room temperature to 500 °C) was attributed to the removal of absorption water and combined water, meanwhile the water vapor produced from dehydration stage contributed the fluctuation. At temperature higher than 500 °C, the reasons for the change of ε_r' value at the latter part were the same as that of manganese anode mud. Similarly, the ε_r' value was observed suddenly to increase to higher levels, with 36.896 (F/M) at 550 °C, which the great increase was attributed to the crystal transformation of amorphous MnO_2 into β-MnO_2; additionally, the decrease of ε_r' value of MnO_2 between 550 °C to 850 °C, was assigned to the deoxidation reaction of $4MnO_2=2Mn_2O_3+O_2$ (g) [35], and the final decrease of the ε_r' value was explained by the deoxidation reaction of $6Mn_2O_3=4Mn_3O_4+O_2$ (g) [35]. While for pure $CaSO_4$ and $PbSO_4$, seen from Fig. 4(c) and Fig. 4(d), the two ε_r' curves presented simple downward trend with temperature increasing, which the downward trend was mainly caused by the removal of absorption water and combined water. The melting point temperature of $PbSO_4$ and $CaSO_4$ phase is 1087 °C and 1450 °C, respectively; hence $CaSO_4$ and $PbSO_4$

phases just occurred a simple dehydration process of absorption water and combined water at temperature ranging from 25 °C to 1000 °C, without chemical reactions. Therefore, it can be concluded from Fig. 4 that the ε_r' value change of manganese anode mud was mainly influenced by the physical and chemical process of MnO_2 phase, with $PbSO_4$ and $CaSO_4$ phase mainly rendering some contribution to the dehydration process of absorption water and combined water.

3.2.2 Dielectric loss factors analysis

Fig. 5 illustrated the dielectric loss factors (ε_r''). ε_r'' refers the substance converts microwave energy into internal energy; meanwhile, ε_r', ε_r'' and tan δ, the three values are related to each other, knowing that two of them can calculate the third value [37-38]. Therefore, the reason for the dielectric constant change can also be applied to explain the change of dielectric loss factor. For manganese anode mud, it was observed from Fig. 5(a) that the ε_r'' value was with a small value of 2.16×10^{-4} (F/M) at room temperature, and increased to 3.453 (F/M) at 100 °C, then having a small drop in the middle with the minimum value of 7.49×10^{-5} (F/M) at 600 °C, then rose to high levels with a value of 3.832 (F/M) at 950 °C, and finally dropped. For the pure MnO_2, as presented in Fig. 5(b), the change trend of ε_r'' values with temperature was generally consistent with that of manganese anode mud, with 1.76×10^{-4} (F/M) at room temperature; beyond 50 °C, it suddenly increased to high levels with 3.574 (F/M) at 50 °C, and those high levels lasted until temperatures higher than 800 °C, with the maximum ε_r'' value of 3.819 (F/M) at 800 °C; higher than 800 °C, the values dropped sharply with temperature. For $CaSO_4$, as shown in Fig. 5(c), the change of ε_r'' values with temperature can be summarized as follows: the maximum value of 5.86×10^{-2} (F/M) was

appeared at room temperature; temperature increasing, the values firstly fell, then rose and next dropped; after temperature exceeding 600 °C, the ε_r'' values of $CaSO_4$ changed slightly. Moreover, it can be seen from Fig. 5(d) that the change of ε_r'' values of $PbSO_4$ with temperature was generally consistent with that of $CaSO_4$, with a maximum value of 5.35×10^{-2} (F/M) at 400 °C. Meanwhile, it can be observed from Fig. 5 that at the same temperature, the ε_r'' values of $CaSO_4$ and $PbSO_4$ were much smaller than that of manganese anode mud and MnO_2, with the difference of two orders of magnitude; while the values of MnO_2 phase were the same order of magnitude as that of manganese anode mud, and the change trend of ε_r'' with temperature for manganese anode mud and MnO_2 was generally consistent. Therefore, it can be concluded from Fig. 5 that MnO_2 phase had more significant effect on the ε_r'' value change of manganese anode mud, compared with the influence of $PbSO_4$ and $CaSO_4$ phase.

3.2.3 Loss tangent coefficients analysis

Fig. 6 showed the loss tangent coefficients (tan δ). tan δ describes the efficiency of the material to convert the absorbed microwave energy into internal energy [37-38]. It can be observed from Fig. 6 that the tan δ curve of each sample showed the same trend with the ε_r'' curve, shown in Fig. 5. Moreover, the change trend of tan δ values of manganese anode mud was generally consistent with that of MnO_2, as shown in Fig. 6(a) and Fig.6(b), respectively; meanwhile, the change trend of tan δ values of $PbSO_4$ was consistent with that of the $CaSO_4$, as shown in Fig. 6(c) and Fig.6(d), respectively. Furthermore, the tan δ values of $CaSO_4$ and $PbSO_4$ at the same temperature were two orders of magnitude smaller than that of manganese anode mud, while the values of MnO_2 phase were the same order of magnitude as that of manganese anode mud, and the change trend of ε_r'' with temperature for MnO_2 phase was

generally consistent with that of manganese anode mud. Hence, the same conclusion can be obtained from Fig. 6, referring to that the tan δ value change of manganese anode mud was mainly influenced by MnO_2 phase.

In summary, it can be concluded from Fig. 4, Fig. 5 and Fig. 6 that the dielectric properties (including ε_r', ε_r'', and tan δ) of manganese anode mud were mainly affected by the physical and chemical process of MnO_2 phase, with $PbSO_4$ and $CaSO_4$ phase mainly rendering some contribution to the dehydration process of absorption water and combined water.

3.3 Microwave heating characteristics analysis

Microwave heating characteristics of materials in microwave field can contribute to verify the correctness of measured dielectric properties of materials. Therefore, the heating characteristics of manganese anode mud and three pure components were investigated in microwave field, as presented in Fig. 7 and Fig. 8, respectively.

Fig. 7 displayed the temperature rise curves of manganese anode mud at different microwave powers. As illustrated in Fig. 7, the heating process of manganese anode mud can be divided into four stages identified by temperatures: <200 °C, 200 °C-700 °C, 700 °C-900 °C, >900 °C, with different temperature rise rates. And with the same tested weight, it took 10.0 min for manganese anode mud to be heated from room temperature to 1000 °C with microwave power at 1000 W, meanwhile with 7.5 min at 1200 W and 5.5 min at 1400 W, respectively, indicating manganese anode mud with excellent microwave-absorbing properties. Meanwhile, it can be concluded from Fig. 7 that with the same objective temperature, increasing microwave power can shorten the heating time. Table

2 introduced the regression parameters in the linear function of temperature, which indicated the relationship between temperature and heating time during microwave heating. Specifically, the function successfully matched the experimental values, with the excellent R^2 (correlation coefficient) values all over 0.97. The slope values of the temperature rise curves revealed the temperature rise rates. Therefore, it can be observed from Table 2 that the temperature rise rate of manganese anode mud at stage II was higher than that of any other stages, with 206.2 °C/min, 276.2 °C/min, and 338.6 °C/min at 1000 W, 1200 W and 1400 W, respectively; which corresponded to the ε_r' change of manganese anode mud with temperature. At temperature increasing from 150 °C to 400 °C, the ε_r' kept at high levels with a maximum value of 20.816 (F/M) at 150 °C and a maximum value of 17.509 (F/M) at 400 °C, both much higher than the ε_r' values at any other temperature range. From the above analysis for Fig. 7 and Table 2, it can be verified that the measured dielectric properties of manganese anode mud was numerically correct.

Fig. 8(a), Fig. 8(b), and Fig. 8(c) showed the temperature rise curves of pure MnO_2, $CaSO_4$ and $PbSO_4$, respectively. As Seen from Fig. 8(a), as heating time prolonged, the heating characteristics of MnO_2 can be divided into four stages identified by different heating rates, with 143.0 °C/min, 291.4 °C/min, 168.0 °C/min, 74.2 °C/min, and 21.0 °C/min. The heating rate at stage II was obviously higher than that of another stage, which was attributed to the crystal transformation of amorphous MnO_2 into β-MnO_2, rendering an increase of ε_r' and further resulting in the higher heating rate at stage II. Moreover, as observed from Fig. 6(a), temperatures exceeding the temperature range of stage II, the heating rate of MnO_2 gradually decreased from 291.4 °C/min to 168.0 °C/min to 74.2 °C/min to 21.0 °C/min, which

was ascribed to the decease of ε_r', caused by the deoxidation reactions of $4MnO_2=2Mn_2O_3+O_2$ (g) and $6Mn_2O_3=4Mn_3O_4+O_2$ (g). As observed From Fig. 8(b), with heating time prolonging, the heating characteristics of $CaSO_4$ was divided into three stages, identified with 10.87°C/min, 6.55 °C/min, and 2.17 °C/min. The gradual decrease of heating rate was caused by the gradual decrease of the ε_r' of $CaSO_4$, which was consistent with the ε_r' curve trend of $CaSO_4$ (Fig. 4(c)). As temperature continually increased, the absorption water and combined water in $CaSO_4$ were gradually removed, rendering the ε_r' value of $CaSO_4$ decreased synchronously. In addition, the heating process of $PbSO_4$ was divided into four stages with 12.29 °C/min, 8.49 °C/min, 3.67 °C/min and 2.96 °C/min (Fig. 8(c)); the decrease of heating rate was also caused by the removal of the absorption water and combined water.

From the above analysis, combined with Fig. 7, Fig. 8 and Table 2, the microwave heating characteristics of manganese anode mud and three pure components successfully matched the dielectric properties change (Fig. 4), verifying the correctness of the measured dielectric properties.

3.4 Phase composition analysis

X-ray diffractometer (XRD) was utilized to characterize the phase transformation of microwave heated manganese anode mud, with 2450 MHz at 1000 °C for 30 min, further to verify the thermal behavior during heating process; and the XRD pattern was presented as Fig. 9.

As observed from Fig. 9, the phase compositions of the microwave treated manganese anode mud contained PbO (JCPDS: 05-0561), Mn_3O_4 (JCPDS: 24-0734), $MnSiO_3$ (JCPDS: 12-0181) and $PbSnF_4$ (JCPDS: 34-1049). In those new generated phases, PbO phase was

generated by the deoxidation reaction of PbO_2 phase, which was produced by the decomposition reaction of lead manganese oxide $Pb_2Mn_8O_{16}$. Moreover, compared with the XRD pattern of the raw manganese anode mud (Fig. 1), it can be concluded that MnO_2 phase in manganese anode mud was reduced into Mn_3O_4 phase, and the peak intensity of the strongest preferential orientation of (101), (101), and (211) plane of Mn_3O_4 phase was observed to appear at 2θ=18.000, 2θ=28.880, and 2θ=36.085, respectively. Moreover, the diffraction peaks of Mn_3O_4 phase were smooth and clear, indicating it with a very good crystalline structure. As new phases, the appearance of PbO and Mn_3O_4 was consistent with the above analysis for the thermal behavior of manganese anode mud. Therefore, the XRD analysis indicated that the analysis of dielectric properties and thermal behavior of manganese anode mud was reasonable.

4 Conclusions

In the present work, the dielectric properties of manganese anode mud and pure MnO_2, $CaSO_4$ and $PbSO_4$ components were measured, and the microwave heating characteristics were determined to verify the relationship between dielectric properties and temperature. The conclusions were summarized as follows:

(1) The thermal behavior of manganese anode mud was divided into five stages: the evaporation of absorption water, removal of combined water, the decomposition reaction of $Pb_2Mn_8O_{16}$ and the deoxidation reactions of PbO_2, MnO_2 and Mn_3O_4.

(2) Manganese anode mud showed excellent responsiveness to microwaves, with high value of ε_r'. And the change of dielectric properties with temperature for manganese anode

mud was related to its thermal behavior. Moreover, the dielectric properties of manganese anode mud were mainly affected by MnO_2 component.

(3) The heating process of manganese anode mud was divided into four stages: <200 °C, 200 °C-700 °C, 700 °C-900 °C, >900 °C, with different temperature rise rates caused by the dielectric properties change. The heating rate of manganese anode mud at the second stage higher than any other stage, attributed to the decomposition reaction of $Pb_2Mn_8O_{16}$ and the crystal transformation of amorphous MnO_2 into β-MnO_2, rendering an increase in dielectric properties. The short heating time for manganese anode mud to be heated from room temperature to 1000 °C, with only 5.5 min, verified that manganese anode mud with excellent microwave-absorbing properties.

Acknowledgments

Financial supports from the National Natural Science Foundation of China (No: U1802255), the Key Projects in the National Science & Technology Pillar Program during the Twelfth Five-year Plan Period (No. 2015BAB17B00), the Hunan Provincial Science and Technology Plan Project, China (No. 2016TP1007), and Innovative Research Team (in Science and Technology) in University of Yunnan Province were sincerely acknowledged.

Appendix A. Supplementary data

Supplementary material related to this article can be found in the online version.

References

[1] B. Sun, F. Fazeli, C. Scott, B.Q. Guo, C. Aranas, X. Chu, M. Jahazi, S. Yue, Microstructural characteristics and tensile behavior of medium manganese steels with different manganese additions, Mater. Sci. Eng. A. 729 (2018) 496-507. https://doi.org/10.1016/j.msea.2018.04.115.

[2] U.S. Mallik, V. Sampath, Influence of aluminum and manganese concentration on the shape memory characteristics of Cu-Al-Mn shape memory alloys, J. Alloy. Compd. 459 (2008) 142-147. https://doi.org/10.1016/j.jallcom.2007.04.254.

[3] R.P. Han, W.H. Zou, Z.P. Zhang, J. Shi, J.J. Yang, Removal of copper(II) and lead(II) from aqueous solution by manganese oxide coated sand I. Characterization and kinetic study, J. Hazard. Mater. 137 (1) (2006) 480-488. https://doi.org/10.1016/j.jhazmat.2006.02.021.

[4] S.S. Tripathy, A.M. Raichur, Abatement of fluoride from water using manganese dioxide-coated activated alumina, J. Hazard. Mater. 153 (3) (2008) 1043-1051. https://doi.org/10.1016/j.jhazmat.2007.09.100.

[5] H. Einaga, A. Ogata, Benzene oxidation with ozone over supported manganese oxide catalysts: effect of catalyst support and reaction conditions, J. Hazard. Mater. 164 (2-3) (2009) 1236-1241. https://doi.org/10.1016/j.jhazmat.2008.09.032.

[6] H. Zhou, H.X. Pan, J.Q. Xu, W.P. Xu, L.F. Liu, Acclimation of a marine microbial consortium for efficient Mn(II) oxidation and manganese containing particle production, J. Hazard. Mater. 304 (2016) 434-440. https://doi.org/10.1016/j.jhazmat.2015.11.019.

[7] J.M. Nan, D.M. Han, M. Cui, M.J. Yang, L.M. Pan, Recycling spent zinc manganese dioxide batteries through synthesizing Zn-Mn ferrite magnetic materials, J. Hazard. Mater. 133(1) (2006) 257-261. https://doi.org/10.1016/j.jhazmat.2005.10.021.

[8] D. Ning, F. Wang, C.B. Zhou, C.L. Zhu, H.B. Yu, Analysis of pollution materials generated from electrolytic manganese industries in China, Resour. Conserv. Recy. 54 (8) (2010) 506-511. https://doi.org/10.1016/j.resconrec.2009.10.007.

[9] Q. Yu, J. Luo, W.Z. Tu, Pollution and its treatment during EMM production, China's Manganese Ind. 24 (3) (2006) 42–5. https://doi.org/10.3969/j.issn.1002-4336.2006.03.013.

[10] S.J. He, T.T. Wei, F.M. Chen, G.L. Li, Application in manganese strata of high-density resistivity prospecting in survey, China's Manganese Ind. 3 (2012) 30-32. https://doi.org/10.3969/j.issn.1002-4336.2012.03.011.

[11] K, Hagelstein, Globally sustainable manganese metal production and use, J. Environ. Manage. 90 (12) (2009) 3736-3740. https://doi.org/10.1016/j.jenvman.2008.05.025.

[12] Y.F. Li, X. Li, H. Ye, X.Z. Kong, Recovery of manganese anode slimes by sulfur reduction roasting-acid leaching process, Nonferrous. Met. 8 (2017) 13-15. https://doi.org/10.3969/j.issn.1007-7545.2017.08.004.

[13] B. Du, C.B. Zhou, X.H. Li, T.Z. Guo, Z.Y. Wang, A kinetic study of Mn(II) precipitation of leached aqueous solution from electrolytic manganese residues, Toxicol. Environ. Chem. 97 (3-4) (2015) 349-357. https://doi.org/10.1080/02772248.2015.1050188.

[14] D.W. Cho, K. Yoon, Y. Ahn, Y.Q. Sun, D.C.W. Tsang, D.Y. Hou, Y.S. Ok, H. Song, Fabrication and environmental applications of multifunctional mixed metal-biochar composites (MMBC) from red mud and lignin wastes, J. Hazard. Mater. 374(2019) 412-419. https://doi.org/10.1016/j.jhazmat.2019.04.071.

[15] I.K.M. Yu, X.N. Xiong, D.C.W. Tsang, L. Wang, A.J. Hunt, H. Song, J. Shang, Y.S. Ok, C.S. Poon, Aluminium-biochar composites as sustainable heterogeneous catalysts for

glucose isomerisation in a biorefinery, Green. Chem. 21(2019) 1267-1281. https://doi.org/10.1039/c8gc02466a.

[16] S.S. Chen, T. Maneerung, D.C.W. Tsang, Y.S. Ok, C.H. Wang, Valorization of biomass to hydroxymethylfurfural, levulinic acid, and fatty acid methyl ester by heterogeneous catalysts, Chem. Eng. J. 328(2017) 246-273. https://doi.org/10.1016/j.cej.2017.07.020.

[17] H.C. Tsai, S.L. Lo, Boron removal and recovery from concentrated wastewater using a microwave hydrothermal method, J. Hazard. Mater. 186 (2-3) (2011) 1431-1437. https://doi.org/10.1016/j.jhazmat.2010.12.010.

[18] C. Yin, J.J. Cai, L.F. Gao, J.Y. Yin, J.C. Zhou, Highly efficient degradation of 4-nitrophenol over the catalyst of Mn_2O_3/AC by microwave catalytic oxidation degradation method, J. Hazard. Mater. 305 (2016) 15-20. https://doi.org/10.1016/j.jhazmat.2015.11.028.

[19] S.Y. Gu, C.T. Hsieh, Y.A. Gandomi, J.K. Chang, J. Li, J.L. Li, H.A. Zhang, Q. Guo, K.C. Lau, R. Pandey, Microwave growth and tunable photoluminescence of nitrogen-doped graphene and carbon nitride quantum dots, J. Mater. Chem. C. 7 (2019) 5468-5476. https://doi.org/10.1039/C9TC00233B.

[20] R.A. Doong, C.Y. Liao, Enhanced visible-light-responsive photodegradation of bisphenol A by Cu, N-codoped titanate nanotubes prepared by microwave-assisted hydrothermal method, J. Hazard. Mater. 322 (2017) 254-262. https://doi.org/10.1016/j.jhazmat.2016.02.065.

[21] J. Feng, Y. Zong, Y. Sun, Y. Zhang, X. Yang, G.K. Long, Y. Wang, X.H. Li, X.L. Zheng, Optimization of porous $FeNi_3$/N-GN composites with superior microwave absorption performance, Chem. Eng. J. 345 (2018) 441-451.https://doi.org/10.1016/j.cej.2018.04.006.

[22] V.H.T. Thi, B.K. Lee, Great improvement on tetracycline removal using ZnO rod-activated carbon fiber composite prepared with a facile microwave method, J. Hazard. Mater. 324 (2017) 329-339. https://doi.org/10.1016/j.jhazmat.2016.10.066.

[23] C. Saucier, M.A. Adebayo, E.C. Lima, R. Cataluña, P.S. Thue, L.D.T. Prola, M.J. Puchana-Rosero, F.M. Machado, F. A..Pavan, G.L. Dotto, Microwave-assisted activated carbon from cocoa shell as adsorbent for removal of sodium diclofenac and nimesulide from aqueous effluents, J. Hazard. Mater. 289 (2015) 18-27. https://doi.org/10.1016/j.jhazmat.2015.02.026.

[24] C. Leonelli, P. Veronesi, D.N. Boccaccini, M.R. Rivasi, L.Barbieri, F. Andreola, I.Lancellotti, D.Rabitti, G.C.Pellacani, Microwave thermal inertisation of asbestos containing waste and its recycling in traditional ceramics, J. Hazard. Mater. 135 (1-3) (2006) 149-155. https://doi.org/10.1016/j.jhazmat.2005.11.035.

[25] G. Chen, L. Li, C.Y. Tao, Z.H. Liu, N. Chen, J.H. Peng, Effects of microwave heating on microstructures and structure properties of the manganese ore, J. Alloy. Compd. 657 (2016) 515-518. https://doi.org/10.1016/j.jallcom.2015.10.147.

[26] Q.X. Ye, J.J. Ru, J.H. Peng, G. Chen, D. Wang, Formation of multiporous MnO/N-doped carbon configuration via carbonthermal reduction for superior electrochemical properties, Chem. Eng. J. 331 (2018) 570-577. https://doi.org/10.1016/j.cej.2017.09.031.

[27] K.Q. Li,, G. Chen, J. Chen, J.H. Peng, R. Ruan, C. Srinivasakannan, Microwave pyrolysis of walnut shell for reduction process of low-grade pyrolusite, Bioresource. Technol. 291 (2019) 121838. https://doi.org/ 10.1016/j.biortech.2019.121838.

[28] X.L. Ye, S.H. Guo, W.W. Qu, L. Yang, T. Hu, S.M. Xu, L.B. Zhang, B.G. Liu, Z.M. Zhang, Microwave field: High temperature dielectric properties and heating characteristics of waste hydrodesulfurization catalysts, J. Hazard. Mater. 366 (2019) 432-438. https://doi.org/10.1016/j.jhazmat.2018.12.024.

[29] K.Q. Li, J. Chen, G. Chen, J.H. Peng, R. Ruan, C. Srinivasakannan, Microwave dielectric properties and thermochemical characteristics of the mixtures of walnut shell and manganese ore, Bioresource. Technol. 286 (2019). https://doi.org/10.1016/j.biortech.2019.121381.

[30] F. He, J. Chen, G. Chen, J.H. Peng, C. Srinivasakannan, R. Ruan, Microwave dielectric properties and reduction behavior of low-grade pyrolusite, JOM. 2019. https://doi.org/10.1007/s11837-019-03522-8.

[31] Tokkan D , S. Kuşlu, T. Çalban, S. Çolak, Optimization of silver removal from anode slime by microwave irradiation in ammonium thiosulfate solutions, Ind. Eng. Chem. Res. 52 (29) (2013) 9719-9725. https://doi.org/10.1021/ie400345g.

[32] R.A. Kuntze, Retardation of the Crystallization of Calcium Sulphate Dihydrate, Nature. 211(5047) (1966) 406-407. https://doi.org/10.1038/211406a0.

[33] J.G. Liu, Z.B. Li, Y.H. Liu, H.S. Yang, L.B. Liang, Study on decomposition dynamics of manganese dioxide, Nonferrous. Met. 12 (2012) 8-12. https://doi.org/10.3969/j.issn.1007-7545.2012.12.003.

[34] X.Y. Guo, H.H. Liu, D. Li, Q.H. Tian, G. Xu, Influence of thermal treatment on the crystal phase transformation of MnO_2, Min. Metall. Eng. 27 (1) (2007) 50-53. https://doi.org/10.3969/j.issn.0253-6099.2007.01.014.

[35] K.T. Jacob, A. Kumar, G. Rajitha, Y. Waseda,Thermodynamic data for Mn_3O_4, Mn_2O_3 and MnO_2, High. Temp. Mat. Pr-isr. 30 (4-5) (2011) 459-472. https://doi.org/10.1515/htmp.2011.069.

[36] Y.X. Hua, C.P. Liu, L. Le, Microwave-assisted decomposition kinetics of MnO_2, Chin. J. Nonferrous. Met. 3 (1998) 497-5091. https://doi.org/10.19476/j.ysxb.1004-0609.1998.03.026.

[37] R.G. Carter, Accuracy of microwave cavity perturbation measurements, IEEE. Trans. Microw. Theory. Tech. 49 (5) (2001) 918–923. https://doi.org/10.1109/22.920149.

[38] M. Santra, K.U. Limaye, Estimation of complex permittivity of arbitrary shape and size dielectric samples using cavity measurement technique at microwave frequencies, IEEE. Trans. Microw. Theory. Tech. 53 (2) (2005) 718-722. https://doi.org/10.1109/tmtt.2004.840570.

Table captions

Table 1 Chemical compositions of manganese anode mud

Table 2 Regression parameters in the linear function of temperature

Figure captions

Fig.1. XRD pattern of raw manganese anode mud

Fig.2. Schematic diagram of (a) dielectric test device and (b) microwave box furnace

Fig.3. TG-DTG-DSC curves of manganese anode mud, (a) TG curves; (b) DTG curves; (c) DSC curves

Fig.4. Dielectric constants (ε_r') of manganese anode mud and three pure components, (a) manganese anode mud; (b) MnO_2; (c) $CaSO_4$; (d) $PbSO_4$

Fig.5. Dielectric loss factors (ε_r'') of manganese anode mud and three pure components, (a) manganese anode mud; (b) MnO_2; (c) $CaSO_4$; (d) $PbSO_4$

Fig.6. Loss tangent coefficients (tan δ) of manganese anode mud and three pure components, (a) manganese anode mud; (b) MnO_2; (c) $CaSO_4$; (d) $PbSO_4$

Fig.7. Microwave heating characteristics of manganese anode mud

Fig.8. Microwave heating characteristics of three pure components, (a) MnO_2; (b) $CaSO_4$; (c) $PbSO_4$

Fig.9. XRD pattern of microwave heated manganese anode mud

Table 1 Chemical compositions of manganese anode mud.

Compositions	Mn	Fe	Pb	CaO	MgO	S	Ni	Co
Mass/W%	57.58	1.06	6.06	7.76	2.52	3.91	0.053	0.021

Table 2 Regression parameters in the linear function of temperature.

Power	Stages	a (°C）	b (°C/min）	R^2
1000 W	I	28.6	100.2	0.98
	II	-120.9	206.2	0.99
	III	296.0	101.0	0.98
	IV	728.0	29.2	0.97
1200 W	I	19.5	14.3	0.99
	II	-116.4	276.2	0.99
	III	316.1	130.4	0.97
	IV	811.3	25.7	0.97
1400 W	I	23.8	157.0	0.98
	II	-145.3	338.6	0.99
	III	352.9	140.8	0.97
	IV	635.6	68.6	0.98

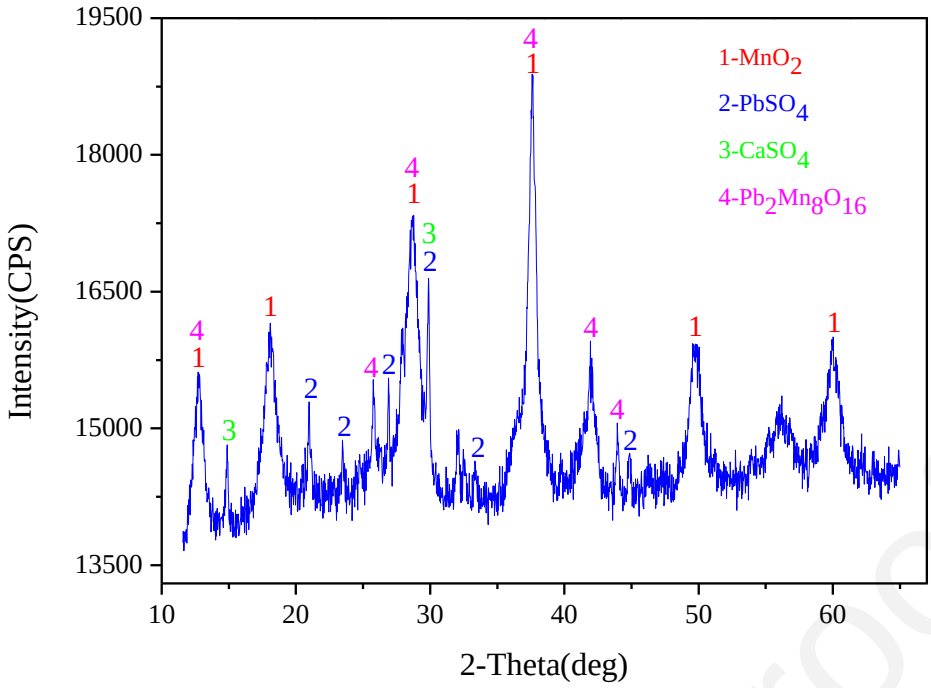

Fig.1. XRD pattern of raw manganese anode mud

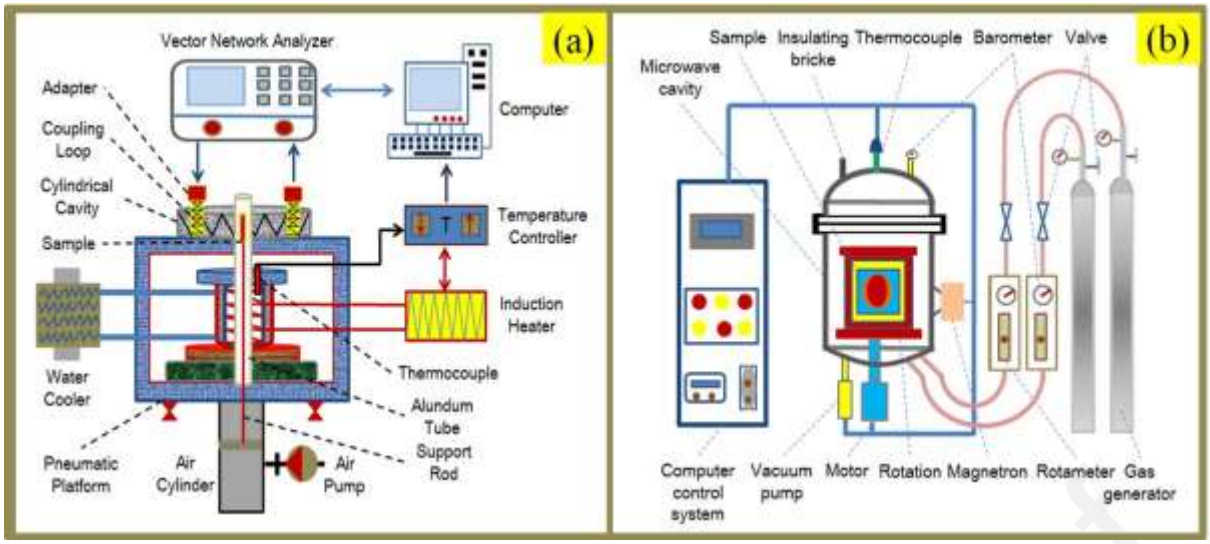

Fig.2. Schematic diagram of (a) dielectric test device and (b) microwave box furnace

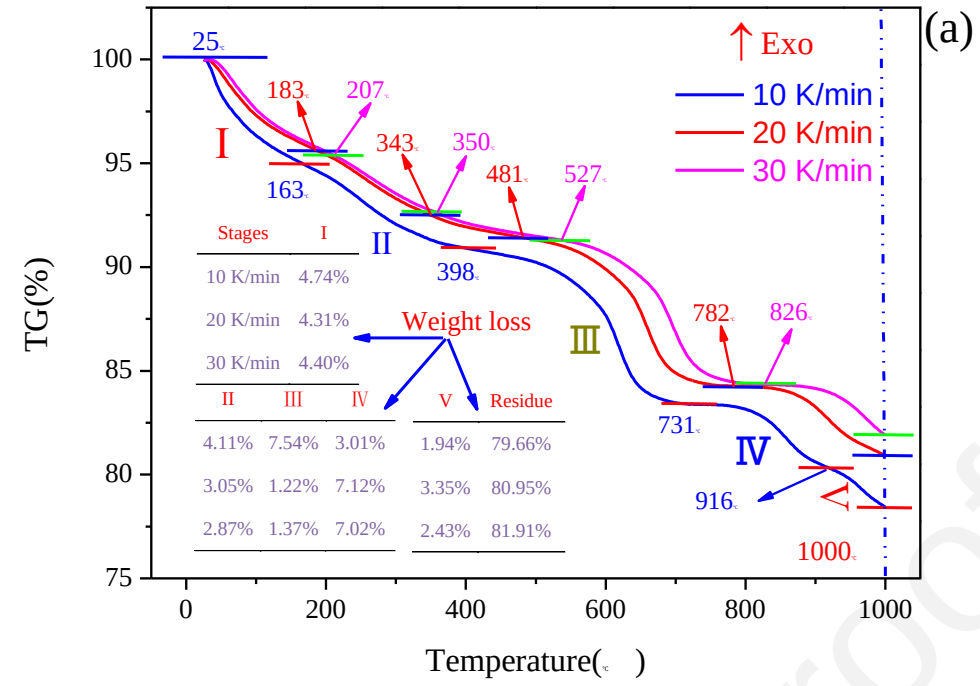

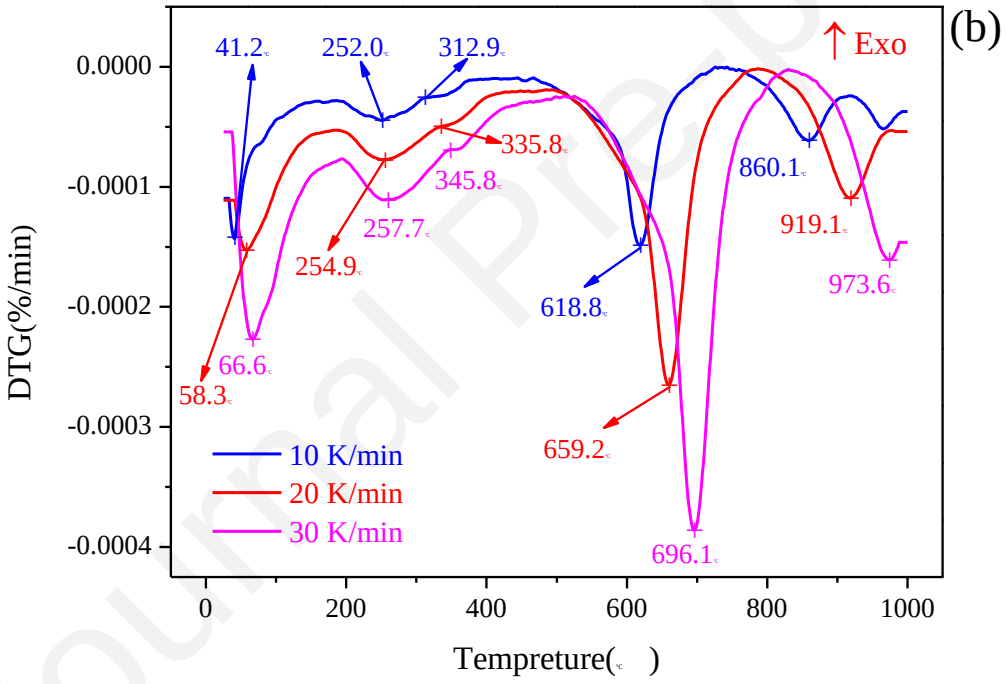

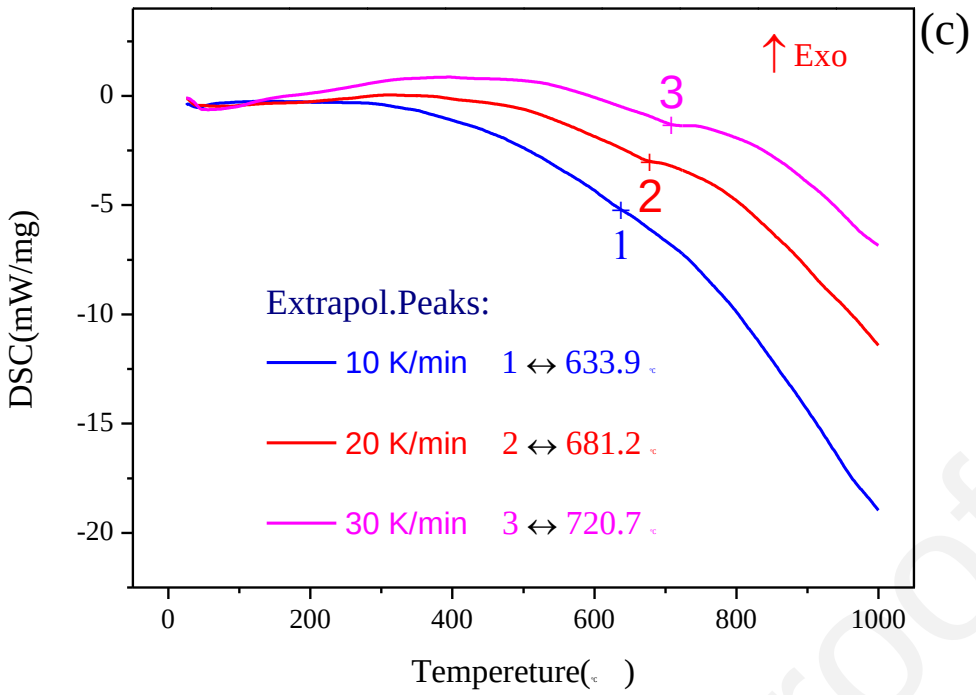

Fig.3. TG-DTG-DSC curves of manganese anode mud, (a) TG curves; (b) DTG curves; (c) DSC curves

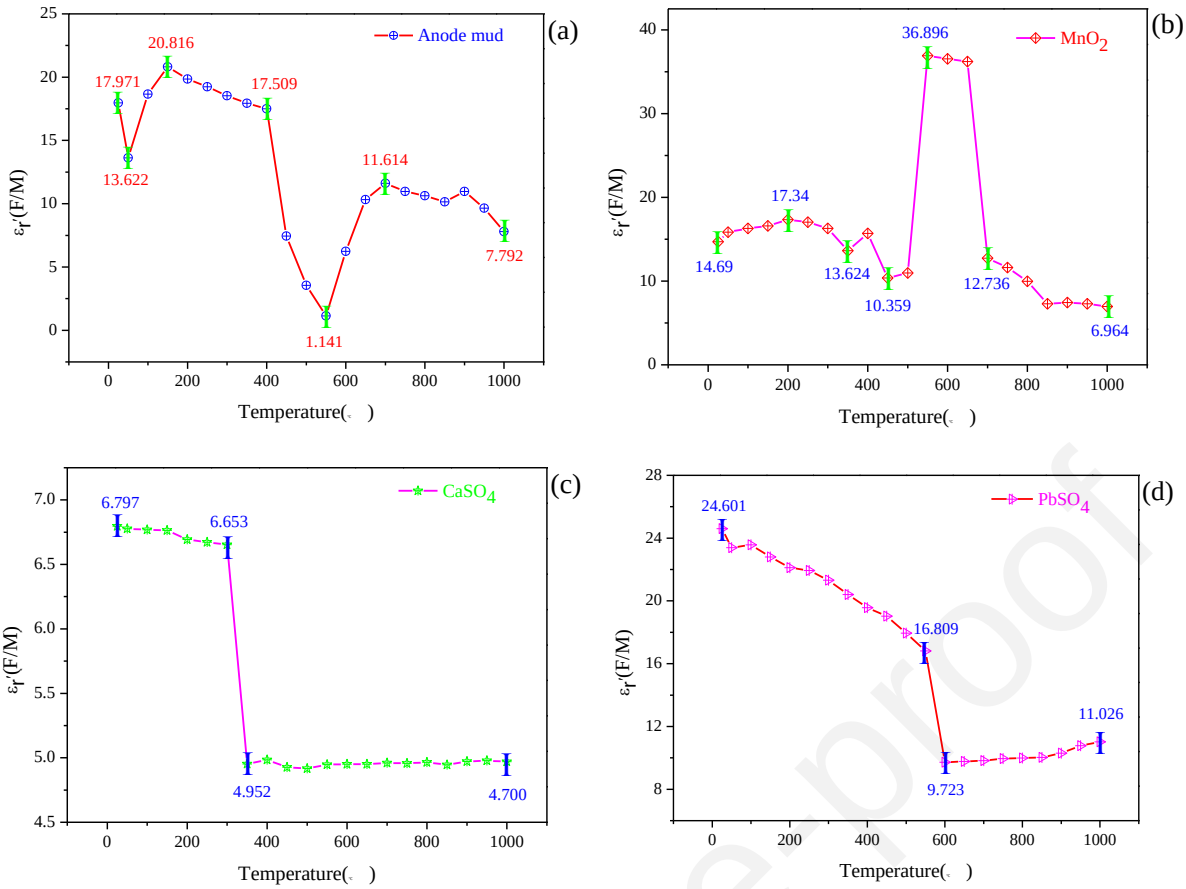

Fig.4. Dielectric constants (ε_r') of manganese anode mud and three pure components, (a) manganese anode mud; (b) MnO_2; (c) $CaSO_4$; (d) $PbSO_4$

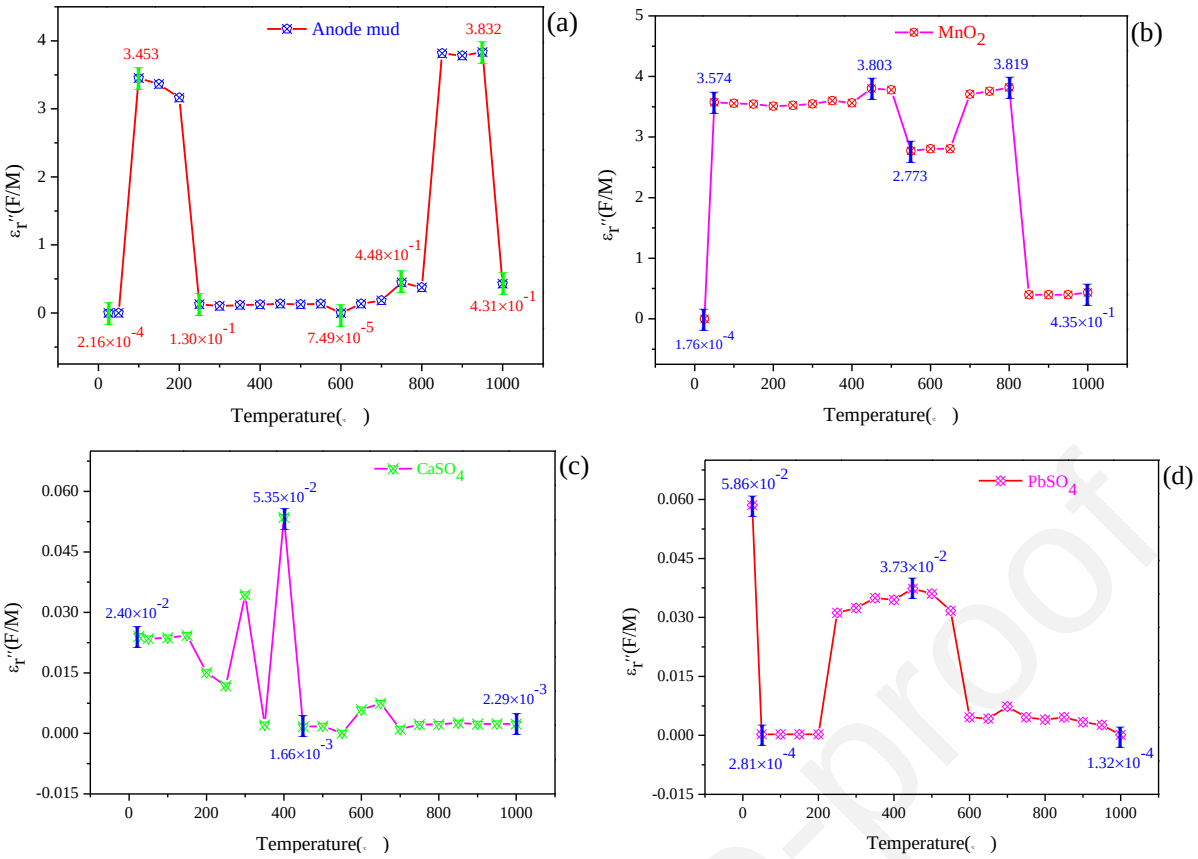

Fig.5. Dielectric loss factors (ε_r'') of manganese anode mud and three pure components, (a) manganese anode mud; (b) MnO_2; (c) $CaSO_4$; (d) $PbSO_4$

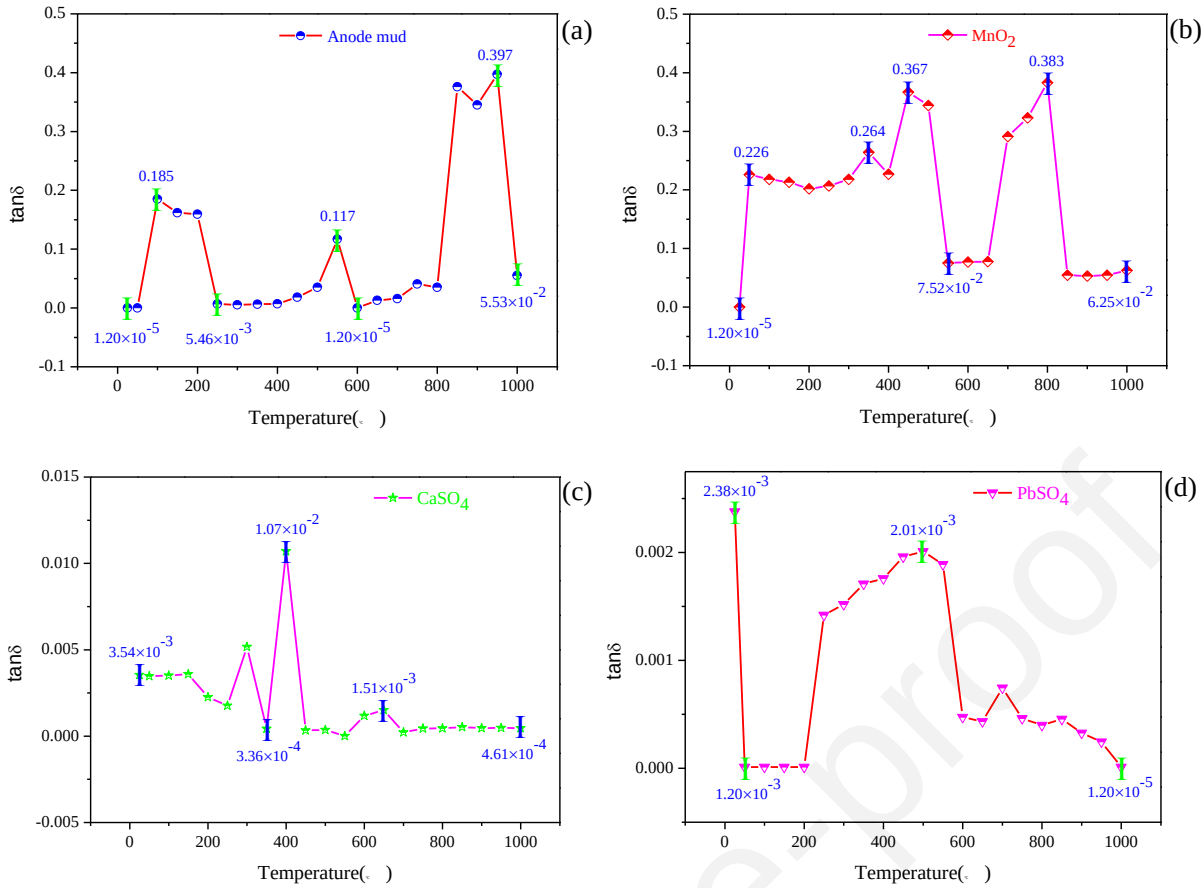

Fig.6. Loss tangent coefficients (tan δ) of manganese anode mud and three pure components, (a) manganese anode mud; (b) MnO_2; (c) $CaSO_4$; (d) $PbSO_4$

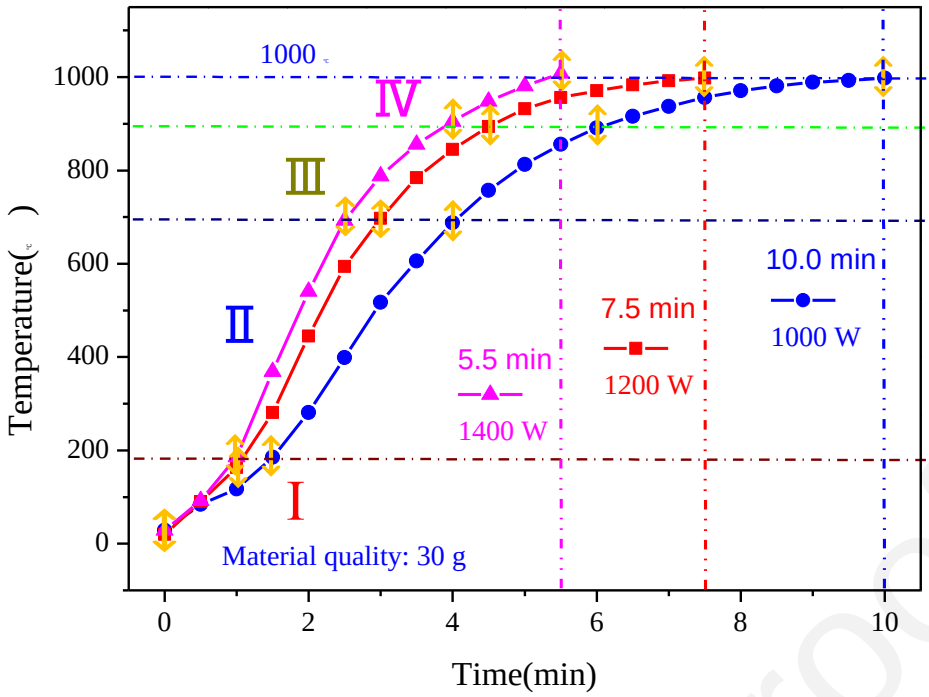

Fig.7. Microwave heating characteristics of manganese anode mud

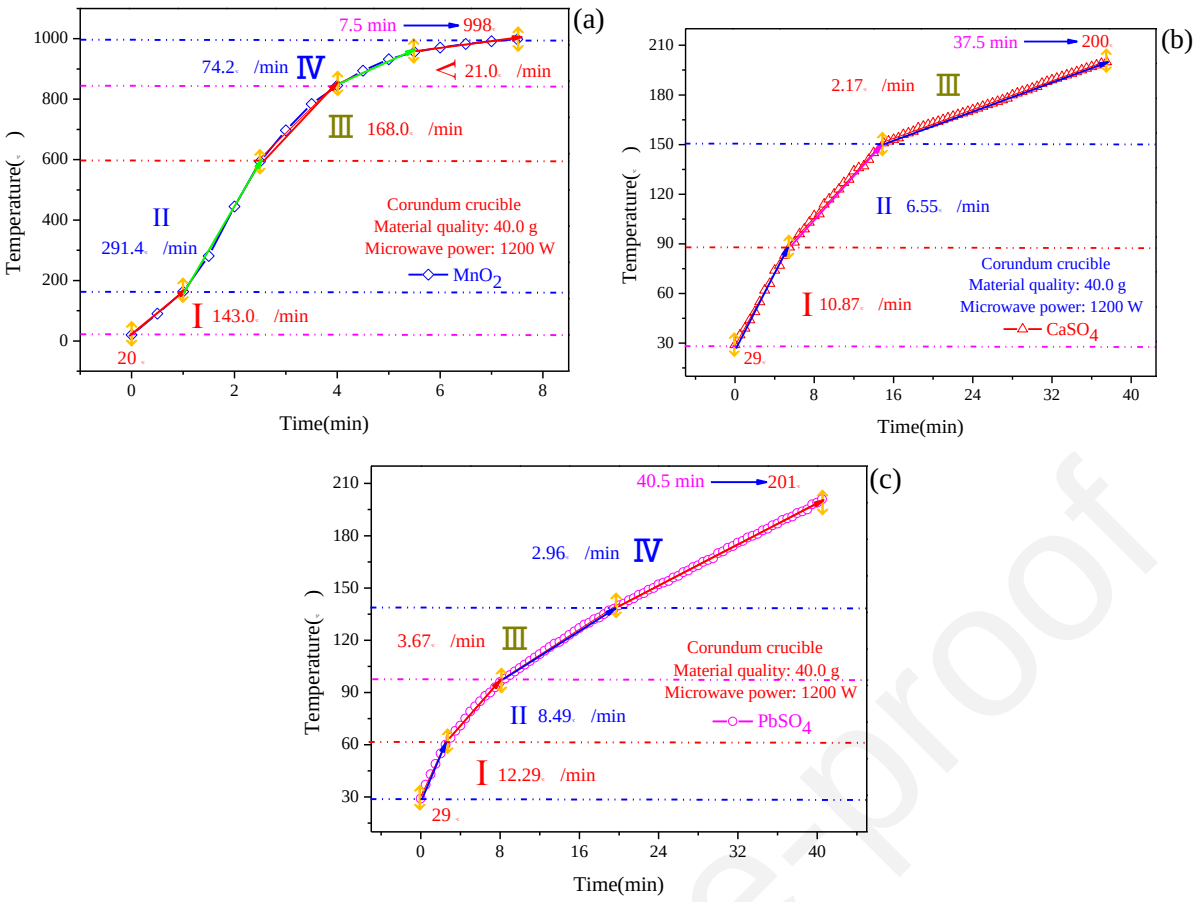

Fig.8. Microwave heating characteristics of three pure components, (a) MnO_2; (b) $CaSO_4$; (c) $PbSO_4$

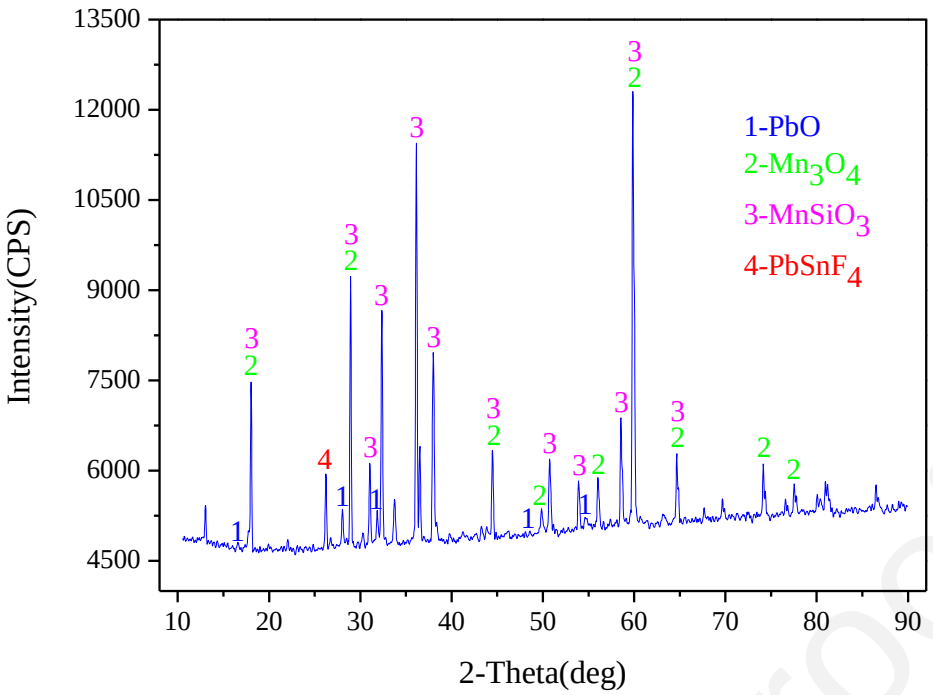

Fig.9. XRD pattern of microwave heated manganese anode mud